Bubble Nucleation During Devolatilization of Polymer Melts

A. L. Yarin
Dept. of Mechanical Engineering, Technion-Israel Institute of Technology, Haifa 32000, Israel

D. Lastochkin, Y. Talmon, and Z. Tadmor
Dept. of Chemical Engineering, Technion-Israel Institute of Technology, Haifa 32000, Israel

Devolatilization of different types of polymer melts was studied experimentally and theoretically. The experimental work was carried out in a ''falling-strand''-type apparatus built especially for this study. Polymer samples after devolatilization were examined by scanning electron microscopy. The micrographs obtained showed that strong nucleation of bubble nuclei occurs first in the vicinity of existing primary microbubbles. These bubble nuclei (secondary nuclei) form blisters (microbubbles) growing under appropriate conditions. The growth is controlled by momentum transfer and diffusion. The microbubbles then coalesce leading to formation of large voids and foaming of the polymer strands. The key parameter, the critical bubble radius triggering the process of growth, was assessed from the micrographs. The time dependence of the concentration of the residual styrene (dissolved gas) in polystyrene melt was determined by gas chromatography. A theoretical model of stress-enhanced secondary nucleation in polymer melts during their devolatilization was developed. It shows that nucleation proceeds due to the growth of initially existing gas bubbles, when a sample is exposed to vacuum. In the vicinity of the bubbles homogeneous nucleation proceeds at an accelerated rate, because it is strongly enhanced by mechanical degradation of polymer macromolecules. The rate of devolatilization was calculated and compared with the experimental data. Theoretical results agreed with the experimental data rather good, although no adjustable parameters characteristic of some of the existing nucleation models were involved.

Introduction

Devolatilization (DV) is an elementary step in polymer processing in which volatile components, for example, unreacted monomers, solvents, or precipitators (such as water), are removed from a polymer after the polymerization reaction step. Devolatilization is carried out to improve product properties, to reach better environmental and health-related standards, and for chemical recovery. Commercial devolatilization involves heating the polymer and reducing the ambient pressure below the equilibrium partial pressure of the volatile component. This phenomenon, which is essentially boiling, is accompanied by bubble formation. Devolatilization, often called ''bubble transport devolatilization,'' is a very complicated process. Its mechanism includes bubble nucleation, their growth due to pressure drop, and molecular diffusion of the dissolved gas, coalescence, and breakup, as well as release of bubble content to the ambient atmosphere.

In industry, DV is carried out in ''falling strand'' devolatilizers or in rotating devolatilizers. The falling-strand devolatilizer consists of a vacuum tank into which polymer melt is extruded in the form of thin strands. By the time the strands reach the bottom of the tank, their volatile content has to be reduced. Falling-strand devolatilizers are often used in the industry when the concentration of a volatile component is relatively high. At lower concentrations rotating devolatilizers based on screw extruders are used. In such machines devolatilization usually proceeds in parallel with polymer compounding by a screw at reduced pressure.

Correspondence concerning this article should be addressed to A. L. Yarin.

In the present work we concentrate first of all on the nucleation of blisters (bubbles) in polymer melts during devolatilization. Therefore literature on bubble nucleation in fluids is of primary importance for us. Nucleation is a physical phenomenon in which a new stable phase is generated within another metastable phase. In this process nuclei are formed due to thermal fluctuations. Those smaller than a critical size are unstable and disappear, whereas those larger than the critical size grow. Such a nucleation is called homogeneous, in contrast to the heterogeneous one, which proceeds due to the presence of some seeds on which supercritical nuclei begin to form.

Many theoretical and experimental studies have been published on bubble nucleation in liquids (most of them deal with low molecular-weight liquids). The review of the early ''classic'' nucleation theories dating back to Gibbs may be found, for example, in books of Frenkel (1945) and Skripov (1974). Later, Blander and Katz (1975) modified the classic nucleation theory for bubble nucleation in a mixture where one component is volatile. They showed that for homogeneous bubble nucleation the nucleation rate, I, can be expressed as

$$I = M(2\sigma/\pi m)^{1/2} \exp(-\Delta F_{cr}/kT), \quad (1)$$

where M is the number of molecules per unit volume of the metastable phase, σ is the surface tension, m is the mass of the gas molecule, k is Boltzmann's constant, T is the temperature, and $\Delta F_{cr} = 16\pi\sigma^3/[3(p_v - p_L)^2]$ is the critical free energy (p_v is the equilibrium vapor pressure and p_L is the liquid pressure; $p_v - p_L$ is often referred to as ''superheat''). Blander and Katz (1975) further modified Eq. 1 for the case of heterogeneous nucleation, accounting for different surface areas and the free surface energies of the liquid–gas, solid–gas, and solid–liquid interfaces. The modified result scales with ΔF_{cr} as follows:

$$I \sim \exp(-F\Delta F_{cr}/kT), \quad (2)$$

where the factor F depends on the contact angle, geometry, and so on. This factor is an empirical adjustable parameter that permits fitting of the theoretical nucleation rate to experimental data. However, such a fitting is not always possible. Moreover, the values of F are not universal and far from the order of one.

It was shown (Lee and Biesenberger, 1989; Han and Han, 1990a,b) that any attempt to apply the classic nucleation theory or its modifications to bubble nucleation in polymer melts leads to temperatures and ''superheats'' far from any plausible estimate. For example, Lee and Biesenberger (1989) in their experiments on a polystyrene/styrene system found the nucleation rates $I \sim \exp(-10^6 \text{ to } -10^8)$ 1/m^3·s for the temperature range 210–250°C. They concluded that formulas for the nucleation rate (homogeneous and heterogeneous) cannot lead to this result at any plausible temperature or ''superheat.'' They also concluded that a better prediction of bubble formation in devolatilization processes is given by assuming heterogeneous nucleation from microscopic cavities (gas pockets) containing gas (for example, those in the extruder walls). Vacuum and supersaturation will cause the gas pockets to grow but not to detach. Only deformation in the melt, generating forces that can overcome surface tension, will be able to free some of the gas entrapped in the cavities and form growing bubble. Such a bubble will continue to grow, leaving a gas pocket in the cavity a source for the next bubble. This type of nucleation was originally suggested by Harvey et al. (1944) for pure liquids of low molecular weight. Lee and Biesenberger (1989) made a small modification in the Harvey model and called it the methastable cavity model (see also Biesenberger and Lee, 1987; Lee, 1991).

Han and Han (1990a) performed a direct experimental study of bubble nucleation phenomena in polymer melts. They worked with an optical cell filled with polystyrene/toluene mixture. They measured the critical nucleus radius (0.24 to 0.32 μm), the critical pressure (pressure when observable nucleation begins), and the nucleation rate by means of light scattering during decompression of the optical cell. Han and Han (1990b) calculated the homogeneous nucleation rate for polystyrene/toluene system based on the experimental data of Han and Han (1990a). They showed that the existing theory of homogeneous nucleation is unable to describe the data. In particular, it predicts practically zero nucleation rate, whereas in reality nucleation in the cell is quite well developed. Given these discrepancies, they proposed a new modified nucleation theory. They included the free-energy change of the solvent due to the presence of macromolecules (according to the Flory-Huggins theory) and the effect of supersaturation. The bubbles are considered to be nucleated not at the thermodynamic equilibrium, so the vapor pressure p_v is not equal to the pressure within the bubble p_g. Their final semiempirical equation scales as

$$I \sim \exp(-\Delta F_{cr}/nkT), \quad (3)$$

where $n \gg 1$ is the number of the solvent molecules in a critical bubble, and

$$\Delta F_{cr} = 16\pi\sigma^3/\left[3(p_v - p_L)^2\right] - nkT \ln(p_g/p_v) - nkT\left(\ln\phi_1 + \phi_2 + \chi\phi_2^2\right), \quad (4)$$

where ϕ_1 and ϕ_2 are the volume fractions of the solvent and solute, and χ is the interaction parameter.

The terms on the righthand side in Eq. 4 are of the order of ΔF_{cr} in Eq. 2. However, after substitution into Eq. 3, they are divided by $n \gg 1$. Therefore Eq. 3 permits us to obtain a nonzero nucleation rate under realistic conditions. However, the calculated theoretical bubble population densities were at least four orders of magnitude larger than the experimental ones. Han and Han (1990b) attributed the discrepancy to possible coalescence in the experiment, which reduces bubble concentration.

Zel'dovich (1942, 1943) in his classic work used as a starting point Gibbs' theory of formation of a new phase. He developed a general microscopical fluctuation approach to calculate the number of the nuclei passing through the critical state under the influence of the negative pressure existing at cavitation. He also assumed that the process is controlled by liquid viscosity, and calculated the nucleation rate in cavitation of Newtonian liquids. The theory of bubble nucleation

during cavitation developed by Zel'dovich (1942, 1943) cannot be directly applied to the devolatilization of polymer melts (as well as any other cavitation theory). However, it contains some general elements that could be useful for a theory of nucleation during devolatilization, which is our aim in the present work.

The survey of the literature in the field of nucleation shows that the existing theories of nucleation (both homogeneous and heterogeneous) cannot be mechanically transplanted to the process of bubble nucleation in polymer melts during their devolatilization. Some general elements of cavitation nucleation theory could be used to develop a new nucleation theory appropriate for the case of devolatilization. Such a theory, however, should inevitably incorporate effects related to the elastic energy of the fluid and the mechanical degradation of macromolecules. Indeed, Albalak et al. (1987, 1990) in their experimental study of devolatilization in a falling-strand devolatilizer showed by SEM that the process is accompanied by rapid nucleation of secondary blisters (bubbles) near the primary ones already existing and growing. They proposed that tensile stresses in the vicinity of the primary bubbles can increase drastically the nucleation rate of the secondary bubbles. In the present work, we shall show that this is, indeed, true, and attribute the effect of the tensile stresses on the nucleation rate to the enhancement of mechanical degradation by these stresses. A theory of such a process should also account for such processes as primary bubble growth. An appropriate approach to this element of the secondary nucleation theory may be taken from the theory of the momentum-controlled (Shulman and Levitsky, 1996) or diffusion-controlled (Scriven, 1959) processes of single-bubble growth in polymer melts.

The present work involves experimental and theoretical study of bubble nucleation during devolatilization of polymer melts. It consists of an experimental part and the theoretical analysis of the nucleation rate in polymer melts in the vicinity of the primary bubbles (where a drastic acceleration of the nucleation is predicted). The theoretical results are discussed and compared with the experimental data.

Experimental Studies

The experimental setup consists of a melt-flow indexer (MFI) (see Figure 1), which melts the polymer pellets, and an evacuated chamber, which is the main part of the system. A thin polymer strand is extruded through the die into the evacuated chamber connected to a rotary vacuum pump and a large vacuum vessel through a liquid-nitrogen trap. The entire system is electrically heated by three heating elements controlled by three independent on–off controllers. The pressure is measured by a digital manometer, which has a response time of less than 20 ms. Polymer pellets are fed into the melt-flow indexer through its funnel-shaped top, and are compressed by a plunger loaded with weights. A controller unit permits us to freeze the molten polymer strand in the chamber at any desired moment by a spray of cooling water through a pneumoelectric valve. The system is equipped with three pneumatically operated vacuum valves. These valves can work at pressures as low as 10^{-9} torr and prevent water-vapor leak into the chamber. They are ''normally closed,'' and open only according to an electric signal from the control box. The

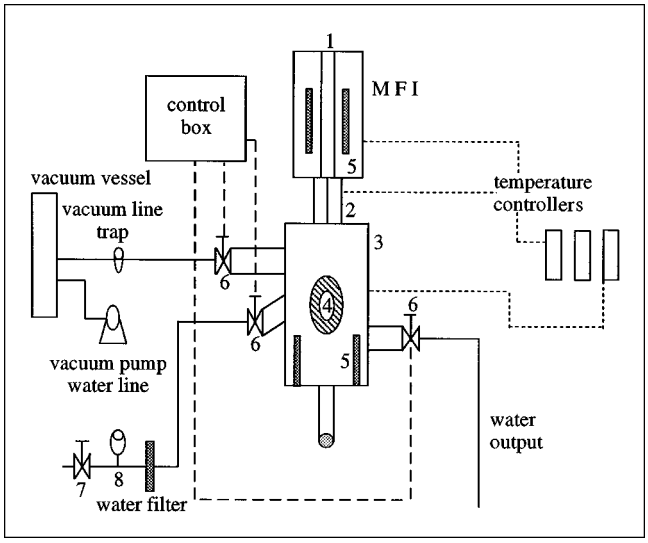

Figure 1. Experimental setup.

(1) Melt-flow indexer; (2) die; (3) vacuum chamber; (4) Pyrex window; (5) heaters; (6) pneumoelectrical valves; (7) water input; (8) water pressure regulator.

valves operate at air pressure of 6 atm. The static pressure of quenching water (2 atm) was set by a water-pressure regulator with differential membrane. The setup is also equipped with a liquid-nitrogen trap for condensation of volatile exhaust and water vapor. All pipe connections are made of 2/3-inch pipes. This diameter provides the identical vacuum at the measuring point and in the chamber. Experiments with HDPE were conducted with a detachable heater and a die of 7 mm diameter. A large vacuum vessel was used because of the short time experiments. System pressure can be estimated by the following equation:

$$p_{sys} = p_{ves} + p_{ch}V_{ch}/V_{ves}, \qquad (5)$$

where subscripts ''ves'' and ''ch'' denote the vessel and chamber, respectively, and p_{ch} is the atmospheric pressure. In order to obtain an ''experimental'' vacuum in the system, which corresponds to p_{sys} close to that of the vessel, p_{ves}, one must operate at a very low V_{ch}/V_{ves} ratio of about 0.001.

After freezing the strands, samples for scanning electron microscopy were prepared. A frozen strand of 3–7 mm in cross section was detached from the die and fractured in liquid nitrogen to reveal its inner structure. The strand pieces were mounted on a special support and gold coated. The specimens were examined in a scanning electron microscope (JEOL5400) in the secondary electron imaging mode. In all the cases a series of five to six micrographs of the same area were taken at magnifications of 35, 100, 350, 1,000, 3,500, and 10,000. These fixed magnification values for all the micrographs of cross-sectional and lateral surfaces of the strands facilitate comparison between different series.

The following materials were used in the present experimental work:

- High-density polyethylene (HDPE)—3,500 to 7,000 ppm volatiles
- ''New'' poly(vinyldifluoride) (PVDF)—20 ppm volatiles

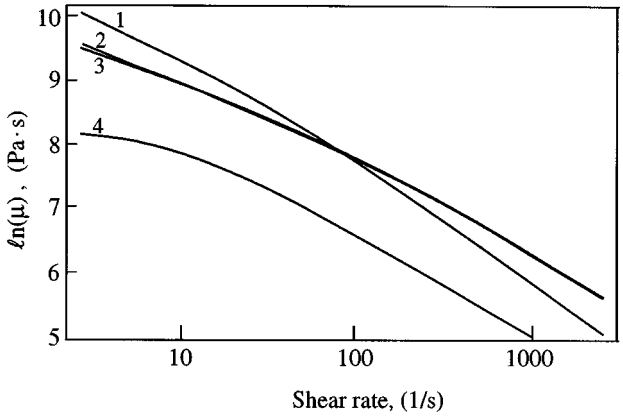

Figure 2. Flow curves of (1) HDPE, $T = 195$°C; (2) "New" PVDF, $T = 235$°C; (3) "Recycled" PVDF, $T = 235$°C; (4) PP, $T = 235$°C.

μ is the shear viscosity.

- "Recycled" poly(vinyldifluoride) (PVDF)—containing 4,000 ppm volatiles
- Polypropylene (PP)—1,500 to 2,000 ppm volatiles
- Polystyrene (PS)—740 to 2,000 ppm of styrene.

The exact nature of the volatiles within the polymers was not known. All the polymers contained a range of substances (for example, the polyolefins contained hydrocarbons from C_4 up to C_{40}). Therefore the analysis of the volatile content after the DV experiments was a complicated task and needed special equipment.

Figure 2 depicts the flow curves of all the polymers at temperatures usually used in polymer processing. The measurements were done using an Instron viscometer with a capillary of 5.1 cm length and 0.126 cm in diameter. All the polymers manifest a characteristic shear-thinning behavior. Note that the viscometer does not allow for measurements for lower shear rates.

In spite of a rather high volatile concentration, HDPE has a very low melt-flow index. The melt-flow index was measured on a ROSAND auto-melt-flow indexer with a load of 216 kg. The following results were obtained: 0.25 g/600 s at 230°C and 0.15 g/600 s at 190°C.

The preliminary experiments on HDPE devolatilization at 200°C showed no foaming in spite of a rather high concentration of volatiles. This was attributed to the high viscosity of HDPE, especially at low shear rates (see Figure 2). Obviously, in the case of an extremely highly viscous polymer, bubbles grow very slowly, and the polymer does not foam during its residence time in the vacuum chamber. The effect of viscosity on the DV process will be discussed below in the theoretical part of the present work.

Figures 3 and 4 illustrate the results obtained for HDPE containing about 5,000 ppm volatiles. The exposure times to vacuum varied from 4.7 s to 46.5 s. DV process is elucidated by Figure 3b, where a number of blisters (bubbles) is clearly seen in the vicinity of a large one. Figures 3c and 3d show the micrographs of the lateral surface of a strand exposed for 4.7 s. At that instant one can observe an important feature: the small bubbles seen on the "ribs" of the large ones. On the macroscopic level (we denote "macro" all the objects larger than 100 μm) macroblisters of the order of 100–500 μm were found (the results are not shown here), while on the microscopic level (less than 100 μm) the microblisters of the order of 0.5–2 μm are observed as a result of nucleation (Figures 3c, 3d). Inside the strand (the results are not shown here) large bubbles of about 1 mm in diameter emerge.

The microstructure of the polymer inside a "fibrous" structure of a big bubble is shown in Figure 4, which depicts the results of the experiment with vacuum exposure time of 10.55 s. Many microblisters expelled volatiles into a large bubble, 2 mm in diameter, as intensive "boiling" occurred. Macroscopical observation of the lateral surface indeed indicated that the strand foamed. The exact nature of the fibrous structure observed on the microscopic level is still an open question. There are two possible explanations: it could simply be a structure induced by freezing of the polymer, or a result of the "boiling" process within the polymer bulk. The latter explanation seems to be more plausible, since in all cases this structure was observed within large bubbles inside polymer strands, and its morphology depended on the time of vacuum exposure only.

From the set of the micrographs of a cross section of a polymer strand exposed to vacuum for 20.55 s (not shown), one can observe microblisters resulting from gas eruption during "boiling" of the polymer melt. Some of those blisters have a crusty appearance. It is interesting that the blistering process in a cross-section of the strand does not end even after 46.5 s of vacuum exposure (Figures 3a, 3b), while the lateral surface does not reveal any blisters at that time. In the cross section of the strand inside the microblisters one can see the characteristic familiar fibrous structures.

A series of experiments were also performed with HDPE enriched with *n*-hexane. The aim of that series was to investi-

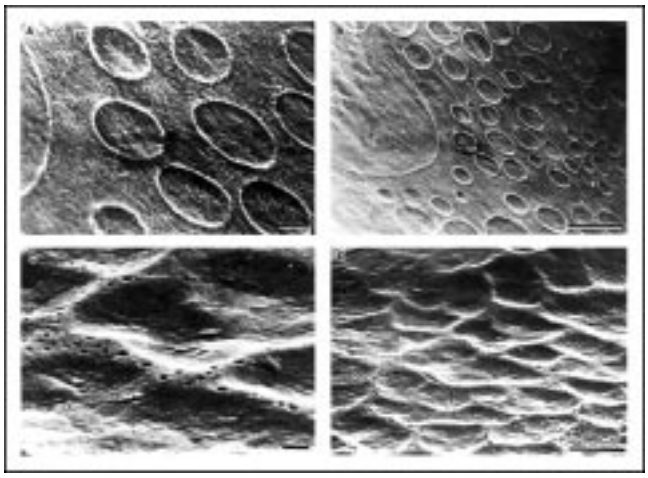

Figure 3. Scanning electron micrographs of a HDPE strand (containing 5,000 ppm volatiles) extruded at 200°C.

(A) Traces of microbubbles in the cross section (subjected to vacuum for 46.5 s, scale bar = 1 μm); (B) traces of microbubbles in the cross section (subjected to vacuum during 46.5 s, scale bar = 5 μm); (C) nucleation on the lateral surface (subjected to vacuum for 4.7 s, scale bar = 1 μm); (D) nucleation on the lateral surface (subjected to vacuum during 4.7 s, scale bar = 5 μm).

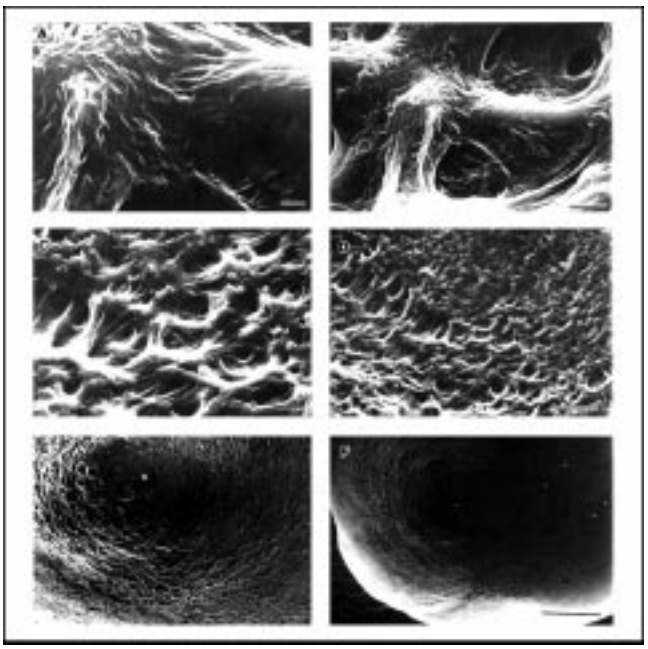

Figure 4. Scanning electron micrographs of the cross section of an HDPE strand (containing 5,000 ppm volatiles) at 200°C and subjected to vacuum for 10.55 s.

The ''boiling'' process within a large void: (A) scale bar = 1 μm; (B) scale bar = 5 μm; (C) scale bar = 10 μm; (D) scale bar = 50 μm; (E) scale bar = 100 μm; (F) scale bar = 500 μm. All are the same area.

gate the effect of volatile concentration on the DV process when the nature of the volatile within the polymer is known. An additional portion of volatiles (an increased volatile concentration) did not change significantly the behavior of the polymer, while a more vigorous foaming was expected.

We also examined devolatilized strands of ''new'' poly (vinyldifluoride) (PVDF) of a very low initial volatile concentration of about 20 ppm. In a sense, this is a rather stringent test of the effectiveness of the system. In spite of a very low volatile concentration, microblisters were clearly seen, evidence that devolatilization has still proceeded.

The DV behavior of the ''recycled'' PVDF was completely different. The polymer foamed quickly and very vigorously, much more than other polymers with comparable or higher volatile content (4,000 ppm for this PVDF).

The experiments with ''recycled'' PVDF showed the strand foaming within the time interval of 0.78 to 4.7 s. Vigorous foaming of this polymer (quite surprising) possessing a rather high viscosity cannot be attributed to high volatile concentration. It may be attributed to a large concentration of nucleation centers in this recycled polymer; however, the most plausible explanation is the decrease of the elastic modulus as a result of recycling process.

In order to observe process dynamics, polypropylene (PP) was exposed in the vacuum chamber for 20.55 s. The relatively low viscosity of PP (see Figure 2) led to strand elongation during the experiment, so that different segments of the PP strand were exposed to vacuum for different periods of time.

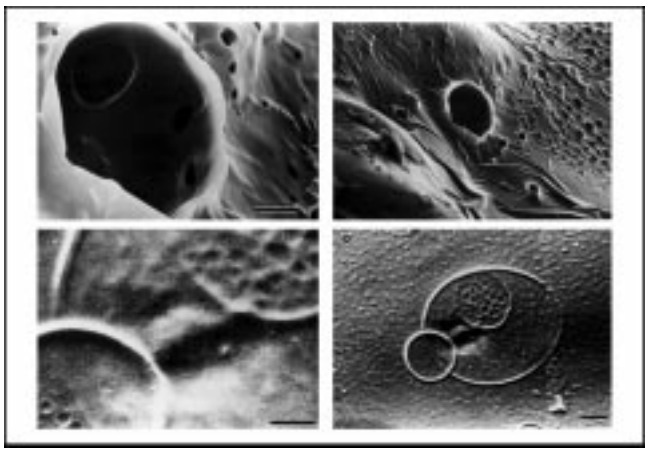

Figure 5. Scanning electron micrographs of the lateral surface of a PP strand (containing 1,500–2,000 ppm volatiles) at 235°C.

(A) Blistering on the lateral surface (subjected to vacuum for 4.7 s; scale bar = 5 μm); (B) blistering and nucleation (subjected to vacuum for 4.7 s, scale bar = 10 μm); (C) coalescing microbubbles (subjected to vacuum during 20.55 s, scale bar = 5 μm); (D) coalescing microbubbles (subjected to vacuum for 20.55 s, scale bar = 10 μm).

Since PP melts have lower viscosity compared to that of HDPE, one would expect a shorter devolatilization process for this polymer. Figures 5c and 5d depict the lateral surface of a PP strand exposed to vacuum for 20.55 s. One can see an example of the coalescence process on the microlevel. Cross-sectional micrographs (not shown) taken at 20.55 s indicate that inside the strand devolatilization is all over. Figures 5a and 5b depict the lateral surface of a PP strand exposed to vacuum for 4.7 s. One can see evidence of ''boiling,'' including the craters caused by the volatile eruption. The smooth lateral surface of the strand indicates that intensive ''boiling'' had already been completed. However, on the microscopic level one can still see growing bubbles. Figures 5a and 5b depict a large number of microblisters on the lateral surface of the strand in the vicinity of a primary growing bubble (crater). The micrographs of the strands exposed for 46.5 s (not shown here) bear clear evidence that the ''boiling'' process is over (cf. with HDPE, where the process is still occurring at 46.55 s).

Figures 6a and 6b show growing microbubbles (craters) on the lateral surface of a PP strand subjected to vacuum for 8.75 s. One can see ''secondary'' nucleated 0.1- to 0.5-μm microbubbles (or microblisters) in the vicinity of the ''primary'' growing 1- to 5-μm microbubbles (craters). This phenomenon was also observed by Albalak et al. (1990) in the polystyrene/styrene system (PS). We extended their data for PS as follows.

It was practically impossible to measure the residual volatile content for the industrial polymers. Therefore a model PS system was used for quantitative measurements of the residual styrene after the DV process. The materials used in the investigation were the industrial polystyrene PS HH102E (supplied by Israeli Petrochemical Enterprises), containing about 740 ppm of residual styrene, and the same material saturated with styrene up to styrene content of about 20,000 ppm.

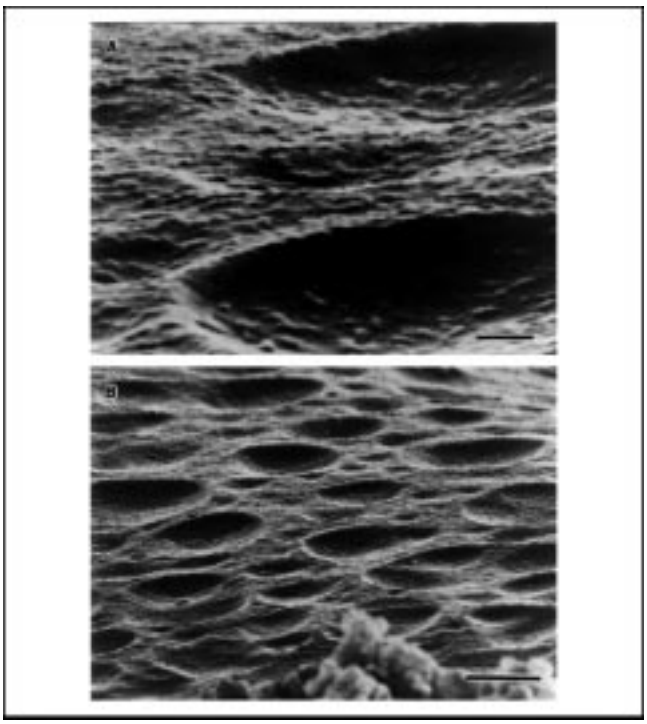

Figure 6. Scanning electron micrographs of the lateral surface of a PP strand (containing 1,500–2,000 ppm volatiles) at 235°C.

(A) Microbubbles (subjected to vacuum for 8.75 s, scale bar = 1 μm); (B) microbubbles (subjected to vacuum for 8.75 s, scale bar = 5 μm).

Figure 7 shows the styrene content evolution with the time of a PS strand. At the onset of vacuum exposure the styrene concentration drops very quickly and after a short time interval reaches a plateau. Every point on the plot represents an average value obtained in several separate experiments.

The samples from the series of experiments conducted with the PS system were checked also by SEM. Figure 8 shows the nucleation process on the lateral surface of the polystyrene

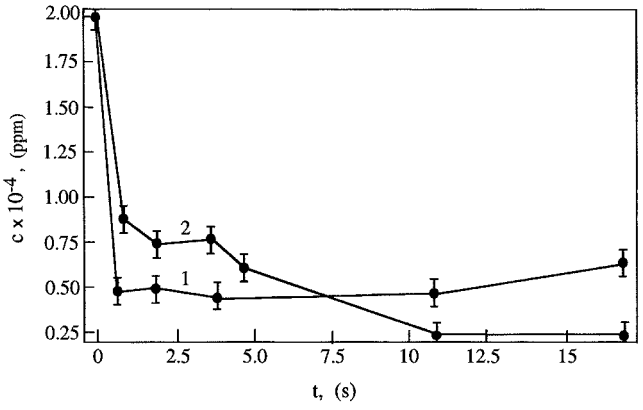

Figure 7. Residual volatile (styrene) concentration in polystyrene vs. time.

(1) The ambient pressure is 1.5×10^{-2} atm; (2) the ambient pressure is 0.75×10^{-3} atm.

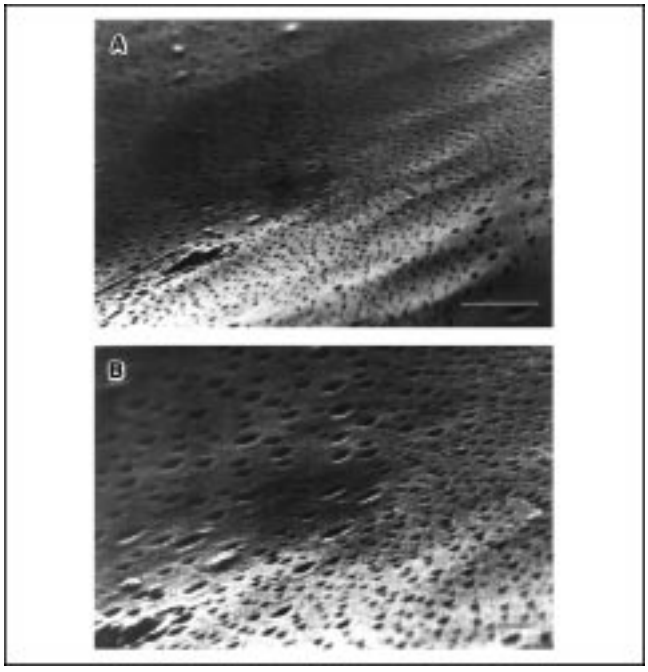

Figure 8. Scanning electron micrographs of a polystyrene strand enriched with styrene (containing 20,000 ppm) at 235°C.

(A) Nucleation on the lateral surface (subjected to vacuum for 1.86 s, scale bar = 1 μm); (B) nucleation on the lateral surface (subjected to vacuum for 1.86 s, scale bar = 5 μm).

strand. Note that the minimal observed size of the nuclei in all the experiments with different polymers, as well as here, was 0.2 to 0.4 μm.

According to the heterogeneous nucleation theory, impurities [for example, dust particles (Albalak et al., 1990)] in the polymer melt may form primary nuclei for bubble growth. In the present work we checked the effect of fine particles on the DV of HDPE samples with TiO_2 powder (1% of powder, the average particle size 0.2 μm). The DV experiments showed that the behavior of ''pure'' HDPE and (HDPE + TiO_2 powder)-system were approximately the same, and the effect of the powder on devolatilization was minor. Although one would expect that a (HDPE + TiO_2)-system should foam quickly and vigorously because of the presence of many primary nuclei, we did not find any evidence of bubble formation on the particles of the TiO_2 powder. Also no evidence of enhanced foaming was observed on the macrolevel.

Theoretical: Nucleation Rate in Polymer Melts

The aim of this section is the prediction of the nucleation rate in polymer viscoelastic melts containing dissolved gas. Such melts consist of a huge number of interpenetrating macromolecular coils. The coils retain their equilibrium shape in a macroscopically stress-free melt at rest. Mutual interaction of macromolecules in concentrated systems (melts, in particular) leads to a force of the order of 3 kT/a acting on a macromolecular coil (Doi and Edwards, 1986; a is the equilibrium subchain length). This force is much less than a typical entropic-elastic force stretching macromolecular coils in a

deformed polymer melt, and we neglect it here. As a result, we can say that there is practically no interaction between equilibrium macromolecular coils. In that case if one coil disappears, the others ''do not feel'' its absence. A hole of the order of the equilibrium macromolecular coil x_0 may emerge or exist in polymer melt at rest, imposing practically no force on its neighborhood. However, this hole may begin to grow after a sample is subject to vacuum. This happens due to the gas pressure inside the hole (if any), or to diffusion of the dissolved gas into it. These processes are referred to as momentum and diffusion controlled, respectively. In any case, due to the growth of these primary bubbles elastic stresses appear in their vicinity. As a result, elastic energy associated with the elastic stresses accumulates in the neighborhood of the hole. If the elastic energy is large enough, mechanical degradation of the neighboring macromolecules will proceed very fast (Yarin, 1991, 1993). If in the vicinity of such a growing hole (a primary bubble) another hole exists (a nucleus of a secondary bubble), it may suddenly begin to grow as a result of a thermal fluctuation. Indeed, its growth is facilitated by a decrease of the accumulated elastic energy due to mechanical degradation. The growth process of the secondary bubble is, however, counteracted by a corresponding increase in its surface energy associated with the surface tension of the polymer melt. However, continuous azimuthal stretching due to the primary bubble growth, and the accumulation of the elastic energy that may be released due to mechanical degradation can allow the secondary bubble to exceed the size of a stable nucleus in spite of surface tension.

As a result, an almost flashlike acceleration of the nucleation rate of the secondary bubbles can occur. As a result of this acceleration, many stable nuclei will appear in the neighborhood of the primary bubble. The resulting blisters (secondary bubbles) then begin to grow due to the internal gas pressure or to diffusion of the dissolved gas, thus leading to an almost explosive disappearance of the whole neighborhood of the primary bubble. (The latter is discussed in detail in the last paragraph of the section on comparison with experimental data.) Due to this mechanism, devolatilization of polymer melts can accelerate drastically and proceed very fast.

Initial stage of growth: Relaxation effects are neglected

We begin calculation of the nucleation rate of the secondary bubbles considering first the primary one (growing due to the momentum transfer or diffusion of the dissolved gas) with the aim of finding the elastic energy stored in its vicinity.

Consider a stress-free hole in polymeric melt. Its radius $x = x_0$ at $t = 0$ grows, and thus $x > x_0$ at $t > 0$. The flow of the melt near the hole is assumed to be radial. Thus from the continuity equation (Bird et al., 1960)

$$\frac{\partial}{\partial r}\left(r^2 v_r\right) = 0 \tag{6}$$

we find

$$v_r = \frac{x^2}{r^2}\frac{dx}{dt}. \tag{7}$$

Here r is the radial coordinate in the spherical coordinate system associated with the center of the hole, v_r is the radial velocity, and we account for the fact that the surface of the hole is a material surface, and thus $v_r = dx/dt$ at $r = x$.

The rate-of-strain tensor D corresponding to the velocity field (Eq. 7) is given by

$$D = \begin{pmatrix} -\frac{2x^2}{r^3}\frac{dx}{dt} & 0 & 0 \\ 0 & \frac{x^2}{r^3}\frac{dx}{dt} & 0 \\ 0 & 0 & \frac{x^2}{r^3}\frac{dx}{dt} \end{pmatrix}. \tag{8}$$

We assume for simplicity that for the entire stretched neighborhood $r \approx x$, and thus

$$D = \begin{pmatrix} -\frac{2\,dx}{x\,dt} & 0 & 0 \\ 0 & \frac{1}{x}\frac{dx}{dt} & 0 \\ 0 & 0 & \frac{1}{x}\frac{dx}{dt} \end{pmatrix}. \tag{9}$$

It is clear that with $dx/dt > 0$ there is compression of the rate $2x^{-1}\cdot dx/dt$ in the radial direction and stretching of the rate $x^{-1}\cdot dx/dt$ in both angular ones.

We assume that the rheological behavior of the melt can be described by the rheological constitutive equation (RCE) of the upper-convected Maxwell liquid (Bird et al., 1977).

$$\frac{d\boldsymbol{\tau}}{dt} = \nabla\boldsymbol{v}\cdot\boldsymbol{\tau} + \boldsymbol{\tau}\cdot\nabla\boldsymbol{v}^T + \frac{2\mu}{\lambda}D - \frac{\boldsymbol{\tau}}{\lambda}, \tag{10}$$

where $\boldsymbol{\tau}$ is the stress tensor deviator, $\nabla\boldsymbol{v}$ is the velocity gradient tensor, μ is the viscosity, and λ is the relaxation time.

It should be noted that the RCE (Eq. 10) describes strong uniaxial elongation of polymeric fluids (the present case) rather well, whereas a more elaborate RCE (see Yarin, 1990, 1993) shows that the viscosity μ in Eq. 10 is related to the zero-shear viscosity μ_0 by

$$\mu = \frac{5}{9}\frac{\mu_0}{N}, \tag{11}$$

where $N \gg 1$ is the number of subchains in a macromolecule.

For the uniaxial elongation we are dealing with $\nabla\boldsymbol{v} = \nabla\boldsymbol{v}^T = D$. Thus using Eq. 9 we find that the radial and the angular components of the deviator (say, τ_{rr} and $\tau_{\theta\theta}$) satisfy the following scalar equations

$$\frac{d\tau_{rr}}{dt} = -\frac{4}{x}\frac{dx}{dt}\tau_{rr} - \frac{4\mu}{\lambda}\frac{1}{x}\frac{dx}{dt} - \frac{\tau_{rr}}{\lambda} \tag{12a}$$

$$\frac{d\tau_{\theta\theta}}{dt} = \frac{2}{x}\frac{dx}{dt}\tau_{\theta\theta} + \frac{2\mu}{\lambda}\frac{1}{x}\frac{dx}{dt} - \frac{\tau_{\theta\theta}}{\lambda}. \tag{12b}$$

For now, we assume for simplicity that the characteristic time of the process is much shorter than the relaxation time, λ, and thus the last terms on the righthand side of Eqs. 12 can be neglected. Then Eqs. 12 are integrated under the conditions $\tau_{rr} = \tau_{\theta\theta} = 0$ at $x = x_0$ ($t = 0$), yielding

$$\tau_{rr} = \frac{\mu}{\lambda}\left[(x_0/x)^4 - 1\right] \tag{13a}$$

$$\tau_{\theta\theta} = \frac{\mu}{\lambda}\left[(x/x_0)^2 - 1\right], \tag{13b}$$

which, as expected, correspond to a nonlinear elastic body of the elastic modulus μ/λ.

Because $x/x_0 > 1$, Eqs. 13 predict $\tau_{rr} < 0$ (radial compression) and $\tau_{\theta\theta} > 0$ (azimuthal stretching).

Assuming that the viscoelastic forces dominate the inertial ones, we can neglect the latter, thus arriving at the momentum equation in the following form (Bird et al., 1960):

$$\frac{\partial p}{\partial r} = \frac{\partial \tau_{rr}}{\partial r} - 2\frac{\tau_{rr} - \tau_{\theta\theta}}{r}. \tag{14}$$

Integrating Eq. 14 over the neighborhood of the hole $r \approx x$, we obtain

$$p = F(t) + \tau_{rr} - 2(\tau_{rr} - \tau_{\theta\theta}), \tag{15}$$

where $F(t)$ is a function found from the boundary condition at the hole surface:

$$-p + \tau_{rr} = -p_b + \frac{2\sigma}{x}. \tag{16}$$

Here σ is the surface-tension coefficient, and p_b is the gas pressure in the hole. The pressure p_b is assumed to be approximately constant at the moment, because the growth of the hole radius is accompanied by the appearance of the products of mechanical degradation inside it. Also diffusion of the dissolved gas is much slower than the radius change at this initial stage of growth.

Substituting Eq. 15 in Eq. 16, we find

$$F(t) = 2(\tau_{rr} - \tau_{\theta\theta}) + p_b - \frac{2\sigma}{x}. \tag{17}$$

Then substituting Eq. 17 in Eq. 15, we find the pressure in the polymer melt near the hole:

$$p = p_b - \frac{2\sigma}{x} + \tau_{rr}. \tag{18}$$

Note that Eq. 18 is an average over the neighborhood $O(x)$ of the primary bubble. If a corresponding pointwise equation would be derived, it should satisfy the condition $p = p_\infty$ at $r = r_\infty$. The latter would allow for description of the dynamics of the bubble evolution, that is, $x(t)$. It is clear that the averaged equation (Eq. 18) cannot be used to find $x(t)$. Fortunately, this is not needed for prediction of the nucleation rate.

Due to Eqs. 13 and 18 the components of the stress tensor $\boldsymbol{\sigma}$ in the neighborhood of the primary bubble are given by

$$\sigma_{rr} = -p_b + \frac{2\sigma}{x} \tag{19a}$$

$$\sigma_{\theta\theta} = -p_b + \frac{2\sigma}{x} + \frac{\mu}{\lambda}\left[(x/x_0)^2 - (x_0/x)^4\right]. \tag{19b}$$

The rate of change of the elastic energy per unit volume, U_e, is given by (Landau and Lifshitz, 1959):

$$\frac{dU_e}{dt} = \boldsymbol{\sigma} : D = \frac{\mu}{\lambda}\frac{2}{x}\frac{dx}{dt}\left[(x/x_0)^2 - (x_0/x)^4\right], \tag{20}$$

(the latter expression is obtained with the help of Eqs. 19 and 8). Equation 20 is integrated subject to the condition $U_e = 0$ at $x = x_0$, which yields

$$U_e = \frac{\mu}{\lambda}\left[(x/x_0)^2 + \frac{1}{2}(x_0/x)^4 - \frac{3}{2}\right]. \tag{21}$$

For simplicity, and as we expect that very rapidly the ratio x/x_0 becomes much larger than 1, we neglect the last two terms on the righthand side of Eq. 21, giving:

$$U_e = \frac{\mu}{\lambda}(x/x_0)^2. \tag{22}$$

Consider now a nucleus of a secondary bubble in the vicinity of the growing primary one. We denote the radius of the nucleus y. The growth of the nucleus triggered by a thermal fluctuation is facilitated by the mechanical degradation (and the corresponding release of the stored elastic energy) in the vicinity of the primary bubble. Therefore, when the nucleus has reached a size y, the corresponding decrease of the free energy due to the mechanical degradation is $-U_e 4\pi y^3/3$. On the other hand, the corresponding increase of the free energy due to the creation of the new free surface is $\sigma 4\pi y^2$. Therefore the free energy is given by

$$\Phi = -\frac{\mu}{\lambda}(x/x_0)^2\frac{4\pi y^3}{3} + 4\pi y^2\sigma \tag{23}$$

(Eq. 22 for U_e has been used).

The critical size of a stable nucleus, y_{cr} corresponds to the condition $d\Phi/dy = 0$, and thus, we find via Eq. 23:

$$y_{cr} = 2\sigma\lambda x_0^2/\mu x^2. \tag{24}$$

According to Zel'dovich (1942, 1943), the rate of formation of such critical nuclei per unit volume, I, is given (in our notation) by

$$I = \frac{1}{\sqrt{2\pi}}\exp\left[-\frac{\Phi|_{y_{cr}}}{kT}\right]\frac{kT}{y_{cr}\mu} \times \sqrt{\left|\frac{d^2\Phi}{dy^2}\right|_{y_{cr}}/kT}\cdot 1/x_0^4. \tag{25}$$

Although Zel'dovich (1942, 1943) considered cavitation in a viscous fluid under negative pressure, it can be easily seen that Eq. 25 is also valid in the present case (cf. the Appendix).

It is emphasized that the argument of the exponential function and the preexponential factor in Eq. 25 are accurate only up to a multiplier of order one, as is common for the existing theories of nucleation.

Substituting Eqs. 23 and 24 into Eq. 25 and neglecting the preexponential factor of order 1, we arrive at the following expression for the nucleation rate of the secondary blisters (bubbles) in the vicinity of the growing primary bubble:

$$I = \exp\left[-\frac{16\pi}{3kT}\frac{\sigma^3\lambda^2 x_0^4}{\mu^2 x^4}\right]\frac{kTx^2}{\sigma\lambda x_0^2}\sqrt{\frac{\sigma}{kT}}\,\frac{1}{x_0^4}. \qquad (26)$$

The latter expression shows that as the radius x of the primary bubble increases, the exponential function in I increases drastically. The latter corresponds to the fact that the growing primary bubble (via stretching in the azimuthal direction) generates elastic energy that may be released by mechanical degradation in its neighborhood. This facilitates the formation of the critical nuclei. As a result, a huge number of the secondary bubbles begin to grow near the primary one, rapidly leading to flash devolatilization of the whole neighborhood via coalesence of the bubbles and formation of a relatively big void. We thus see that the primary bubbles that begin to grow when a sample is exposed to vacuum can, in principle, trigger an avalanche-like process of nucleation and growth of the secondary bubbles in their vicinity.

Taking the following characteristic values of the polymer parameters: $\sigma = 2\times10^{-2}$ N/m, $\lambda = 1$ s, $\mu = 10^5$ Pa·s, $x_0 = 10^{-7}$ m, $k = 1.38\times10^{-23}$ J/K, and $T = 500$ K, we estimate the nucleation rate of the secondary bubbles. (Note that the initial size of the hole is estimated as the end-to-end size of a random walk of N freely jointed Kuhn segments b, $x_0 = bN^{1/2}$. Typically for polymer macromolecules $N \sim 10^4$, $b \sim 10^{-9}$ m, and thus $x_0 \sim 10^{-7}$ m). Therefore the nucleation rate of the secondary blisters is given as per Eq. 26, as $I \approx 1.01973\times10^{32}\exp(-6.2422\times10^{-22}/x^4)x^2$. The values of this function are presented in Table 1. They show that beginning from the primary bubble size, x, of several microns one should expect a significant nucleation rate of secondary bubbles.

Table 1. Nucleation Rate of the Secondary Bubbles as per Eq. 26

Bubble Size x, μm	Nucleation Rate I, 1/m^3·s
0.1	~ 0
1	~ 0
2	4.65×10^{3}
3	4.13×10^{17}
4	1.42×10^{20}
5	9.39×10^{20}
6	2.26×10^{21}
10	9.58×10^{21}
100	1.02×10^{24}

Effect of relaxation in the melt on the nucleation rate of the secondary bubbles

In the previous subsection we considered only the very initial stage of the process, when relaxation of the elastic stresses can be neglected. It permits us to obtain relatively simple analytical expressions and to estimate the nucleation rate of the secondary blisters. This rate, however, tends to infinity as $t\to\infty$ and $x\to\infty$. The latter points out that at times comparable to the relaxation time of the melt, stress relaxation should be accounted for. In the present subsection we take stress relaxation into consideration.

At an early stage of a primary bubble growth its radius evolves approximately as

$$x = x_0\exp(t/\alpha), \qquad (27)$$

where α is a characteristic time for the momentum-controlled process of bubble growth. Note that this expression follows from the Rayleigh-Plesset equation for bubble radius (Leal, 1992) when the inertial effects are negligibly small.

Substituting Eq. 27 into Eq. 12, we obtain the following equations for the components of the stress tensor deviator

$$\frac{d\tau_{rr}}{dt} = -\frac{4}{\alpha}\tau_{rr} - \frac{4\mu}{\lambda}\frac{1}{\alpha} - \frac{\tau_{rr}}{\lambda} \qquad (28a)$$

$$\frac{d\tau_{\theta\theta}}{dt} = \frac{2}{\alpha}\tau_{\theta\theta} + \frac{2\mu}{\lambda}\frac{1}{\alpha} - \frac{\tau_{rr}}{\lambda}. \qquad (28b)$$

The solutions of these equations (with $\tau_{rr} = \tau_{\theta\theta} = 0$ at $t = 0$) are

$$\tau_{rr} = \frac{4\left[-1+\exp\left(-\frac{4t}{\alpha}-\frac{t}{\lambda}\right)\right]\mu}{\alpha+4\lambda} \qquad (29a)$$

$$\tau_{\theta\theta} = -\frac{2\left[-1+\exp\left(\frac{2t}{\alpha}-\frac{t}{\lambda}\right)\right]\mu}{\alpha-2\lambda}, \qquad (29b)$$

which after substitution of $t = \alpha\ln(x/x_0)$, yields

$$\tau_{rr} = \frac{4\left[-1+(x/x_0)^{-\alpha/\lambda}x_0^4/x^4\right]\mu}{\alpha+4\lambda} \qquad (30a)$$

$$\tau_{\theta\theta} = \frac{\left[2-2(x/x_0)^{-\alpha/\lambda}x^2/x_0^2\right]\mu}{\alpha-2\lambda}. \qquad (30b)$$

As expected, the solutions (Eqs. 30) reduce to Eq. 13 when $\lambda \gg \alpha$.

The rate of change of the specific elastic energy is thus given by (Yarin, 1991, 1993):

$$\frac{dUe}{dt} = -\frac{8\mu\left[-1+x_0^4(x/x_0)^{-\alpha/\lambda}/x^4\right]dx/dt}{(\alpha+4\lambda)x} + \frac{2\mu\left[2-2x^2(x/x_0)^{-\alpha/\lambda}/x_0^2\right]dx/dt}{(\alpha-2\lambda)x} - \frac{U_e}{\lambda}. \qquad (31)$$

The solution of Eq. 31, subject to the initial condition $U_e = 0$ when $x = x_0$ at $t = 0$, is

$$U_e = -\left[2e^{[-t(\alpha+4\lambda)/\alpha\lambda]}\mu\{(-1+e^{6t/\alpha})\alpha + 2\lambda(1+2e^{6t/\alpha}-3e^{t(4/\alpha+1/\lambda)})\}\right]/[(\alpha-2\lambda)(\alpha+4\lambda)]. \quad (32)$$

In terms of the primary bubble radius the specific elastic energy is found using Eqs. 27 and 32 as follows:

$$U_e = -\left[2\mu\left\{\alpha\left(-1+(x/x_0)^{6/\alpha}\right)+2\lambda\left(1+2(x/x_0)^{6/\alpha} - 3(x/x_0)^{4/\alpha+1/\lambda}\right)\right\}(x/x_0)^{-4/\alpha-1/\lambda}\right]/[(\alpha-2\lambda)(\alpha+4\lambda)]. \quad (33)$$

Thus, similarly to Eq. 23, we find the free energy

$$\Phi = -U_e\frac{4\pi y^3}{3} + 4\pi y^2\sigma. \quad (34)$$

The critical size of the nucleus corresponds to $d\Phi/dy = 0$:

$$y_{cr} = -\frac{(\alpha-2\lambda)(\alpha+4\lambda)\sigma(x/x_0)^{4/\alpha+1/\lambda}}{\mu\left[\alpha\left(-1+(x/x_0)^{6/\alpha}\right)+2\lambda\left(1+2(x/x_0)^{6/\alpha}-3(x/x_0)^{4/\alpha+1/\lambda}\right)\right]}. \quad (35)$$

The free energy corresponding to the critical size y_{cr} is given by

$$\Phi_{cr} = \frac{4\pi(\alpha-2\lambda)^2(\alpha+4\lambda)^2\sigma^3(x/x_0)^{2(4/\alpha+1/\lambda)}}{3\mu^2\left[\alpha\left(-1+(x/x_0)^{6/\alpha}\right)+2\lambda\left(1+2(x/x_0)^{6/\alpha}-3(x/x_0)^{4/\alpha+1/\lambda}\right)\right]^2}. \quad (36)$$

Thus, using Eq. 25 we arrive at the expression for the nucleation rate of the secondary bubbles in the vicinity of the growing primary one:

$$I = -\left\{2e^{-\psi}\left[\alpha\left(-1+(x/x_0)^{6/\alpha}\right)+2\lambda\left(1+2(x/x_0)^{6/\alpha}-3(x/x_0)^{4/\alpha+1/\lambda}\right)\right](x/x_0)^{-4/\alpha-1/\lambda}\right\}/\left[(\alpha-2\lambda)(\alpha+4\lambda)\sqrt{\sigma/kT}\,x_0^4\right] \quad (37a)$$

$$\psi = \frac{4\pi(\alpha-2\lambda)^2(\alpha+4\lambda)^2\sigma^3(x/x_0)^{2(4/\alpha+1/\lambda)}}{3kT\mu^2\left[\alpha\left(-1+(x/x_0)^{6/\alpha}\right)+2\lambda\left(1+2(x/x_0)^{6/\alpha}-3(x/x_0)^{4/\alpha+1/\lambda}\right)\right]^2}. \quad (37b)$$

This result is valid at a relatively early stage of the primary bubble growth, since it is based on Eq. 27. In the present analysis we choose polymer relaxation time as the characteristic time of the process. So we fix the relaxation time and vary the growth rate of the primary bubble. One can easily see that the stresses actually depend on the ratio α/λ. The radial and azimuthal stresses for several values of α are shown for a fixed $\lambda = 1$ s in Figure 9. In all the cases presented $\alpha > 2\lambda$, and the azimuthal stresses approaches a finite value, as it should be for the upper-convected Maxwell fluid. From the expression for the azimuthal stresses one can see that for $\alpha < 2\lambda$ the azimuthal stresses infinitely grow with time, which is also known for the upper-convected Maxwell fluid. Note that for $\alpha = 2\lambda$ the azimuthal stress grows linearly as $\mu t/\lambda^2$.

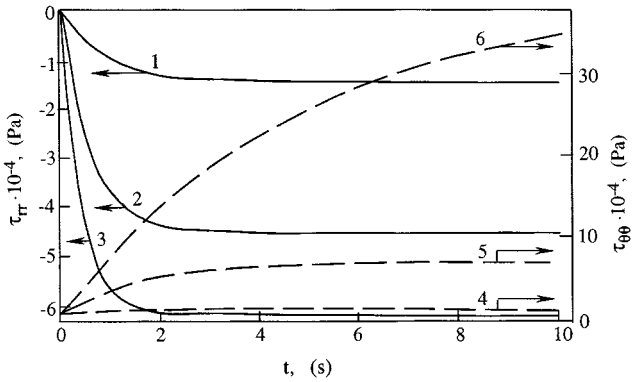

Figure 9. Radial and azimuthal stresses near the surface of the primary bubble at $\mu = 10^5$ Pa·s and $\lambda = 1$ s.

The radial stresses: (1) $\alpha = 25$ s; (2) $\alpha = 5$ s; (3) $\alpha = 2.5$ s. The azimuthal stresses: (4) $\alpha = 25$ s; (5) $\alpha = 5$ s; (6) $\alpha = 2.5$ s.

According to Eqs. 37 there is practically no nucleation when $\alpha > 2\lambda$, corresponding to slow growth of the primary bubble. Indeed, for $\alpha = 2.5$ s even at a very large $x = 10^{-2}$ m (remember that the nucleation rate increases with the primary bubble growth), the nucleation rate is negligibly small, 4.33×10^{-77816}. On the other hand, for $\alpha < 2\lambda$ (corresponding to fast growth of the primary bubble) we obtain a very significant nucleation rate at appropriate values of the bubble radius. An example for $\alpha = 0.5$ s is presented in Table 2.

As expected, we obtain considerable nucleation rate only in the case of sufficiently fast primary bubble growth. Therefore we can expect a significant nucleation rate only at the

Table 2. Secondary Nucleation Rate as per Eq. 37

Bubble Size x, μm	Nucleation Rate I, 1/m^3·s
0.5	9.03×10^{-11}
0.6	8.46×10^{10}
0.8	6.06×10^{19}
1	2.61×10^{21}
2	6.15×10^{22}
3	2.11×10^{23}
4	5.01×10^{23}
5	9.79×10^{23}
6	1.69×10^{24}

beginning of the primary bubble growth. After a certain time, when the growth rate of the primary bubble decreases, nucleation should decelerate due to the effect of stress relaxation. In the present case we do not observe a decrease of the nucleation rate in Table 2, since we chose Eq. 27 as the bubble growth law.

Note also that the nucleation rate is extremely sensitive to the value of the elastic modulus of the melt, since at the onset of the bubble growth the process is controlled by momentum transfer and hence by the elastic modulus of the melt.

Uniformly valid expression for the rate of secondary nucleation

In the previous subsection we obtained an approximate expression for the nucleation rate of secondary bubbles, assuming that the primary bubble grows exponentially as per Eq. 27, which is valid only at an early stage of the process. The aim of the present subsection is to obtain a uniformly valid description of the rate of the secondary nucleation. We now use the theory of a single (primary)-bubble growth, which is uniformly valid at any time (and not only at a relatively early stage as Eq. 27). Such a theory was developed, for example, by Shulman and Levitsky (1996) and modified in Lastochkin (1998). In this case, the expressions for the radial and azimuthal stresses in the vicinity of the primary bubble are given by

$$\tau_{rr} = -\frac{4\mu}{\lambda}\frac{e^{-t/\lambda}}{R(t)^4}\int_0^t e^{\xi/\lambda}R(\xi)^3R'(\xi)\,d\xi \qquad (38a)$$

$$\tau_{\theta\theta} = \frac{2\mu}{\lambda}e^{-t/\lambda}R(t)^2\int_0^t \frac{e^{\xi/\lambda}R'(\xi)}{R(\xi)^3}\,d\xi, \qquad (38b)$$

where R is the current bubble radius, and the primes indicate differentiation according to the corresponding variable. The equation for the rate of change of the elastic energy in the present case reads (cf. Yarin, 1991, 1993)

$$\frac{dU_e}{dt} + \frac{U_e}{\lambda} = \frac{4\mu}{\lambda}(I_1 + I_2) \qquad (39a)$$

$$\frac{dI_1}{dt} = -\frac{I_1}{\lambda} - 5I_1\frac{R'(t)}{R(t)} + \frac{2R'(t)^2}{R(t)^2} + I_1\frac{R''(t)}{R'(t)} \qquad (39b)$$

$$\frac{dI_2}{dt} = -\frac{I_2}{\lambda} + I_2\frac{R'(t)}{R(t)} + \frac{R'(t)^2}{R(t)^2} + I_2\frac{R''(t)}{R'(t)}, \qquad (39c)$$

where

$$I_1 = \frac{2e^{-t/\lambda}}{R(t)^5}R'(t)\int_0^t e^{\xi/\lambda}R(\xi)^3R'(\xi)\,d\xi \qquad (40a)$$

$$I_2 = e^{-t/\lambda}R(t)R'(t)\int_0^t \frac{e^{\xi/\lambda}R'(\xi)}{R(\xi)^3}\,d\xi. \qquad (40b)$$

It may be shown that for $t \ll \lambda$ Eqs. 39 and 40 reduce to Eq. 21, with x/x_0 replaced by $R(t)/R(0)$.

Using Eq. 34, the critical size of the nucleus, the free energy, and its second derivative corresponding to the critical size of the nucleus, as well as the general expression for the nucleation rate, may be written as follows

$$y_{cr} = 2\sigma/U_e \qquad (41a)$$

$$\Phi|_{y_{cr}} = 16\pi\sigma^3/3U_e^2 \qquad (41b)$$

$$\left.\frac{d^2\Phi}{dy^2}\right|_{y_{cr}} = -8\pi\sigma \qquad (41c)$$

$$I = \exp\left(-\frac{16\pi\sigma^3}{3kTU_e^2}\right)\sqrt{\frac{\sigma}{kT}}\,\frac{kTU_e}{\mu\sigma R_0^4}. \qquad (41d)$$

Numerical implementation of Eqs. 39 is simpler and we proceed with it. In the case of the momentum-driven bubble growth, the bubble radius $R(t)$ and its derivatives can be found from the theory of Shulman and Levitsky (1996), which supplements Eqs. 39 and 40 and permits us to obtain the specific elastic energy, the primary bubble radius, and the pressure within the bubble as functions of time.

Note that in the case of the diffusion-driven bubble growth, the system of Eqs. 39 and 40 is supplemented by the solution of Scriven (1959) for the bubble radius modified in Lastochkin (1998).

We also assume that all the secondary bubbles grow according to the same growth law. So the mass of the gas within the growing secondary bubbles at time t is obtained as follows:

$$c^*(t) = \frac{4\pi}{3}\int_0^t I(t-\tau)\frac{R^3(\tau)\,p(\tau)\,M}{\rho R_g T}\,d\tau, \qquad (42)$$

where p, ρ, and T are the pressure, the density, and the temperature (remember that we deal with an isothermal process) of the gas within the bubbles; M is the molecular mass of the gas; R_g is the gas constant; and the gas is assumed to be ideal. The fraction of the residual volatile content in the melt that can be experimentally measured is defined as

$$\text{Dev} = 1 - \frac{c^*(t)}{c_0}, \qquad (43)$$

where c_0 is the initial mass of the dissolved gas in the sample.

The dimensionless form of the governing equations is given by

$$\frac{dU_e^*}{dt} = -U_e^* + H_1 + H_2 \tag{44a}$$

$$H_1' = \frac{2SR'(t)^2}{R(t)^2} - \Big\{H_1\Big[R(t)^2\big(J_1'(t) + J_2'(t) + p'(t)\big) + S(-1+\beta)R(t)R'(t) + 2R'(t)\big(\sigma^* - 2SR'(t) + 2S\beta R'(t)\big)\Big]\Big\} \Big/ \{S(-1+\beta)R(t)R'(t)\} \tag{44b}$$

$$H_2' = \frac{SR'(t)^2}{R(t)^2} - \Big\{H_2\Big[R(t)^2\big(J_1'(t) + J_2'(t) + p'(t)\big) + S(-1+\beta)R(t)R'(t) + 2R'(t)\big(\sigma^* + SR'(t) - S\beta R'(t)\big)\Big]\Big\} \Big/ \{S(-1+\beta)R(t)R'(t)\} \tag{44c}$$

$$\frac{d}{dt}\big\{p(t)R(t)^3\big\} = \frac{6DeFu^2[1-p(t)]^2R(t)^4}{\big[p(t)R(t)^3 - 1\big]} \tag{44d}$$

$$-p(t) + \frac{2\sigma^*}{R(t)} + p_\infty = J_1(t) + J_2(t) - \frac{S(1-\beta)R'(t)}{R(t)} \tag{44e}$$

$$J_1'(t) + J_1(t)\left[1 + \frac{4R'(t)}{R(t)}\right] = -\frac{S\beta R'(t)}{2R(t)} \tag{44f}$$

$$J_2'(t) + J_2(t)\left[1 + \frac{R'(t)}{R(t)}\right] = -\frac{S\beta R'(t)}{2R(t)}, \tag{44g}$$

with the following dimensionless variables and parameters involved:

$$U_e^* = \frac{U_e}{p_{b0}} \tag{45a}$$

$$\sigma^* = \frac{\sigma}{p_{b0}R_0} \tag{45b}$$

$$Fu = \frac{\rho R_g T}{Mk_h} \tag{45c}$$

$$De = \frac{D\lambda}{R_0^2} \tag{45d}$$

$$S = \frac{4\mu}{\lambda p_{b0}} \tag{45e}$$

$$p(t) = \frac{p_b}{p_{b0}} \tag{45f}$$

$$H_1 = \frac{2e^{-t}S\left[\int_0^t e^{\xi}R(\xi)^3R'(\xi)\,d\xi\right]R'(t)}{R(t)^5} \tag{45g}$$

$$H_2 = e^{-t}S\left[\int_0^t \frac{e^{\xi}R'(\xi)}{R(\xi)^3}\,d\xi\right]R(t)\,R'(t). \tag{45h}$$

Here D is the diffusion coefficient; p_b is the pressure within the primary bubble; p_{b0} and R_0 are the initial pressure within the primary bubble and its initial radius; and k_h is the Henry constant. Bars over the dimensionless time t and the dimensionless bubble radius $R(t)$ are omitted. Note that the physical origin of Eq. 44d is the mass balance of gas in a bubble. The mass changes due to the mass flux into the bubble, which is given by the righthand side of Eq. 44d. This mass flux was calculated using distribution of gas concentration outside the bubble. The latter was found using the gas concentration at the bubble surface that depends on pressure via Henry's law. Therefore the Henry constant appears in Eq. 45c. Parameter β governs contribution of the Maxwell element into the effective viscosity.

The secondary nucleation rate Eq. 41d is thus given in the form:

$$I = \exp\left[-\frac{16\pi p_{b0}R_0^3(\sigma^*)^3}{3kT(U_e^*)^2}\right]\sqrt{\frac{p_{b0}R_0\sigma^*}{kT}}\,\frac{kTU_e^*}{\mu R_0^5\sigma^*} \tag{46}$$

Results, Discussion, and Comparison with Experiment

Nucleation rate: General trends

First we check the predictions of the present theory using some characteristic values of the parameters involved, to evaluate the qualitative behavior of the results. We take the following values of the parameters: $\sigma = 2\cdot10^{-2}$ N/m; $\mu = 10^5$ Pa·s, $R_0 = 2\cdot10^{-7}$ m, $p_{b0} = 2\cdot10^5$ Pa, $D = 4\cdot10^{-10}$ m^2/s, and $T = 500$ K. Obviously, the devolatilization efficiency, that is, the ratio of the residual gas content to the initial one, must be less than 1. In other words, the amount of the gas that the growing bubbles can absorb from the polymer melt does not exceed the initial volatile content. We calculate the specific elastic energy, the nucleation rate, and the degree of devolatilization, neglecting possible coalescence of the secondary bubbles.

The specific elastic energy corresponding to the relaxation time $\lambda = 0.825$ s and the corresponding nucleation rate are shown in Figure 10. At the onset of the process the growing primary bubble creates azimuthal stresses in its vicinity that accelerate nucleation of the secondary bubbles, and thus the nucleation rate, I, sharply increases. After a certain time, however, stress relaxation predominates, leading to a decrease of the specific elastic energy in the surrounding polymer melt. As a result, the nucleation rate of the secondary bubbles decreases sharply after $t = 4$, as seen in Figure 10.

Figure 10 shows that the devolatilization process is actually a steplike process, since the nucleation rate is extremely sensitive to variations of the specific elastic energy. Therefore the process of the secondary nucleation proceeds only in a narrow time interval. Accordingly, for any comparable value of λ, the residual volatile content in the melt drops sharply in a steplike manner, as seen in Figure 11 at about $t = 5$.

As expected, the residual volatile content in the melt is strongly affected by the relaxation time, which governs the relaxation of the elastic stresses, and thus the specific elastic energy and the secondary nucleation rate.

Figure 12 shows the effect of the diffusion Deborah number De (cf. Eq. 45d), or the diffusion coefficient, on the specific elastic energy and the secondary nucleation rate. Obvi-

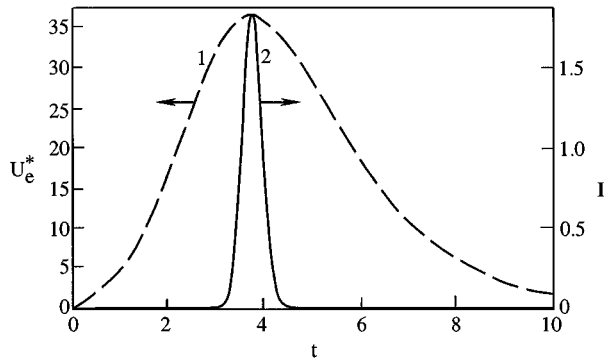

Figure 10. (1) Specific elastic energy for $\lambda = 0.825$ s (the dashed line); (2) secondary nucleation rate as a function of time (the solid line).

Time is rendered dimensionless by λ; the dimension of I is $10^7/m^3 \cdot s$.

ously, an increase in the diffusion coefficient enhances bubble growth rate and hence increases drastically the secondary nucleation rate.

Comparison with experimental data

Here we compare the theoretical results with the experimental data we obtained for the PS system. The experiments were performed at 235°C. The material parameters available in the literature correspond to 230°C and 250°C (see Tables 3 and 4). The values of the parameters at $T = 235$°C needed in the present section were linearly interpolated from Tables 3 and 4 and were taken to be as follows: the Henry's constant $k_h = 24.7$ atm, the melt density $\rho = 0.692$ g/cm^3, and the surface tension $\sigma = 9.95$ dyne/cm.

Note that in the present subsection we use Henry's law in the form $p = k_h c$, where the Henry constant k_h is taken in the pressure units. The other material properties are given in Table 5. The key parameter, namely the initial bubble radius, $x_0 = 0.2$ μm, was directly measured in our experiments, which completely agrees with the results of the study of bubble nucleation during decompression of the polystyrene/toluene mixture (Han and Han, 1990a). Our experimental result agrees with the estimate of x_0 as the end-to-end random walk size in the theoretical part, where we obtained $x_0 \sim 10^{-7}$ m $= 0.1$ μm.

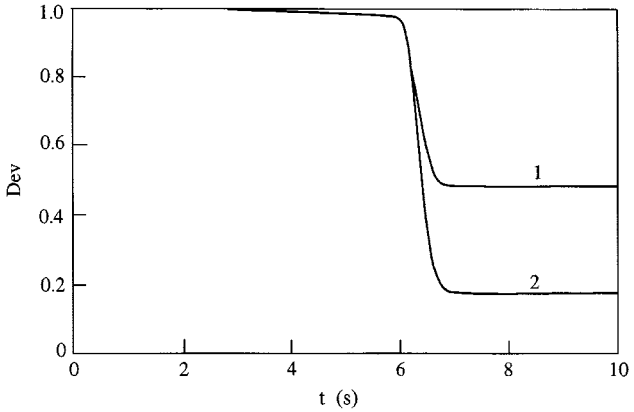

Figure 11. Residual volatile content in the melt as a function of time for the two values of the relaxation time: (1) $\lambda = 0.827$ s, and (2) $\lambda = 0.828$ s.

Time is rendered dimensionless by the values of λ, different for the two curves shown.

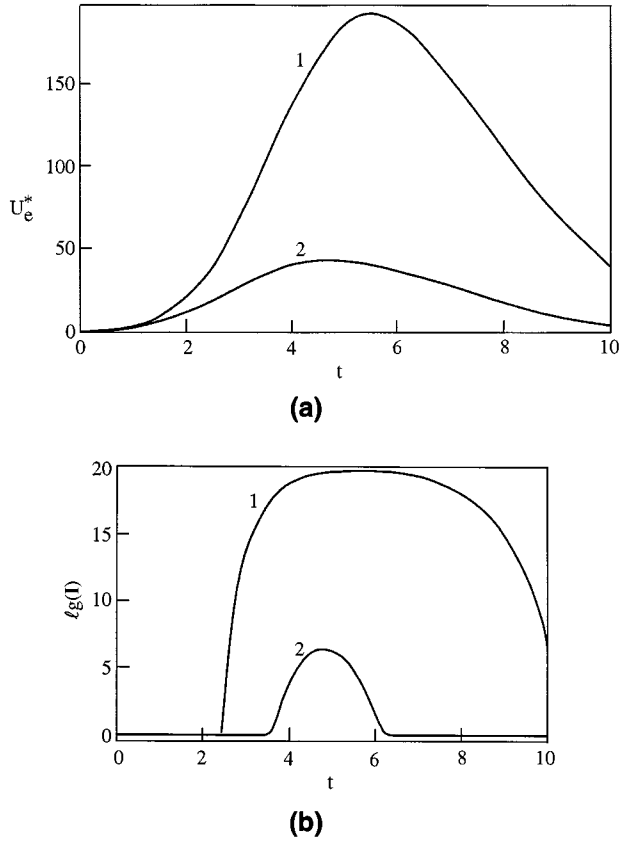

Figure 12. Effect of the Deborah number on the specific elastic energy and the nucleation rate.

(1) $De = 2.5 \times 10^4$; (2) $De = 2.5 \times 10^3$ (time is rendered dimensionless by $\lambda = 0.825$). (A) Specific elastic energy. (B) The corresponding secondary nucleation rate.

We use a relatively high value of viscosity (see Table 5), because we deal with the extensional flow, which is typically "shear thickening."

The main result of the previous theoretical section is that devolatilization efficiency characterized by the devolatilization degree, Dev, drops fast at a certain instant and then reaches a plateau (cf. Figure 11). This is also clearly seen in the experimental data of Figure 7, replotted here in terms of *Dev* (see Figure 13).

The volume of the secondary bubbles in a unit volume increases during the devolatilization process as

Table 3. Material Properties of the Polystyrene/Styrene Systems at 230°C

Parameter	Value
Henry's constant	21.5 atm
Melt density	0.70 g/cm^3
Surface tension	10.4 dyne/cm

Source: After Lee and Biesenberger (1989).

Table 4. Material Properties of the Polystyrene/Styrene System at 250°C

Parameter	Value
Henry's constant	34.8 atm
Melt density	0.67 g/cm^3
Surface tension	8.6 dyne/cm

Source: After Lee and Biesenberger (1989).

$$V_{\text{sec bub}}(t) = \frac{4\pi}{3}\int_0^t I(t-\tau)\,R^3(\tau)\,d\tau \qquad (47)$$

(and the volume of the melt decreases as $V_{\text{melt}}(t) = 1 - V_{\text{sec bub}}$, respectively).

According to the percolation theory (Stauffer, 1979, 1985), at approximately $V_{\text{sec bub}} = 0.7$ the secondary bubbles coalesce, the melt foams, and the devolatilization process is essentially finished. Thus the duration of the devolatilization process, the cutoff time, t^*, is found from the condition $V_{\text{melt}}(t^*) = 0.3$. At that instant the calculations corresponding to the results shown below were stopped.

The nucleation rate for the PS system at 235°C is calculated by Eq. 41d:

$$I = 1.04923\times 10^{18}\exp\left[-\frac{58{,}859.3}{(U_e^*)^2}\right]U_e^*. \qquad (48)$$

The residual volatile content is found by Eq. 47. The fact that in the experiments the ambient pressure is low but finite, and even time-dependent, has only a minor effect on the results. The results obtained for $\lambda = 0.825$ s and $\lambda = 0.7$ s show that the residual gas content drops sharply at the very beginning of devolatilization close to $t = 0$ s and then reaches a plateau. The results of the calculations also show that at lower λ, and thus higher elastic modulus, devolatilization starts after a certain time delay (for example, there is practically no devolatilization until $t = 3$ s, for $\lambda = 0.65$ s). At a certain λ ($\lambda = 0.6$ s and less) there is no devolatilization (which means that t^* tends to infinity).

The theoretical results are compared to the experimental data in Figure 13. The general trends are similar and the values are rather close even though no adjustable parameters (like F introduced by Blander and Katz, cf. Eq. 2) are involved. Note that this has been achieved by taking the relaxation time λ of the order of 1 s (0.7 s and 0.825 s). Relaxation time λ roughly corresponds to the reciprocal shear rate, where the shear thinning begins to be felt (Yarin, 1990, 1993). For the polystyrene it yields $\lambda \sim 1$ s, which is close enough to the values of λ fitting the data in Figure 13. Therefore the "fitting" effect of λ is incomparably less than that of F in Eq. 2, and λ actually is not an adjustable parameter.

Table 5. Additional Material Properties of the Polystyrene/Styrene System

Parameter	Value
Diffusion coefficient	4.07×10^{-10} m^2/s
Viscosity	10^5 Pa·s
Initial styrene concentration	20,000 ppm
Styrene molecular weight	104 g/mol

Note: The diffusion coefficient is taken from Yang and Smith (1997), the initial styrene concentration and the molecular weight correspond to the experiments.

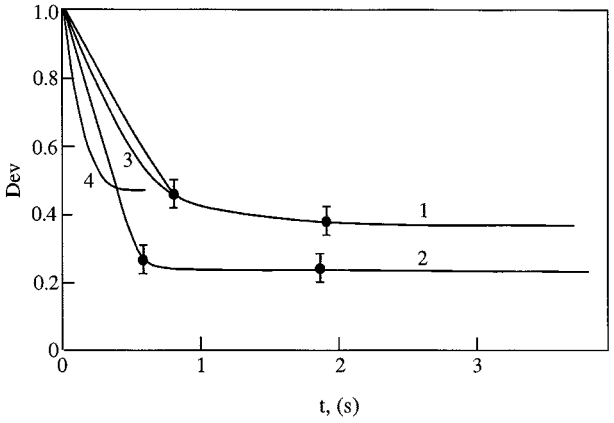

Figure 13. Comparison with the experimental data.

(1) and (2) The experimental data for 0.75×10^{-3} atm and 1.5×10^{-2} atm, curves 1 and 2, respectively; theoretical results: (3) $\lambda = 0.7$ s, $t^* = 7.15$; (4) $\lambda = 0.825$ s, $t^* = 3.25$ ($\mu = 10^5$ Pa·s).

For the applications it is of interest to estimate a duration of devolatilization and the effect of rheological properties of the melt on it. The theory of the present work allows us to do that. The duration of the devolatilization process as a function of the relaxation time λ is shown in Figure 14. When the relaxation time decreases at a fixed viscosity the duration of the devolatilization process increases, because the elastic modulus increases. Note, however, that beginning at a certain value the relaxation time becomes so short and the elastic stresses relax so fast that the secondary nucleation is practically arrested.

An increase of the zero-shear viscosity μ at a constant relaxation time also leads to an increase of the elastic modulus of the melt, and as a result, to deceleration of devolatilization. This is illustrated in Figure 15.

The results shown in Figures 13 to 15 were obtained for the diffusion coefficient $D = 4.07\times 10^{-10}$ m^2/s. At higher values of the diffusion coefficient its effect on the duration of devolatilization diminishes and becomes negligibly small, as

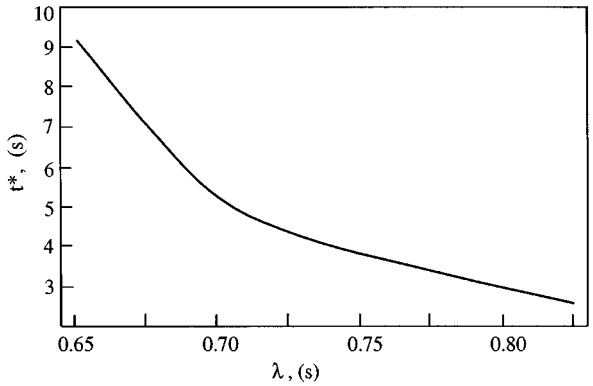

Figure 14. Effect of the polymer relaxation time on the duration of the devolatilization process: T = 235°C, $\mu = 10^5$ Pa·s.

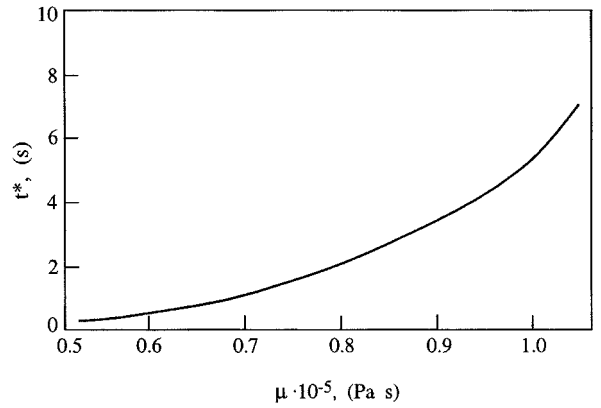

Figure 15. Effect of viscosity variation of the melt on the duration of the devolatilization process at a fixed relaxation time $\lambda = 0.7$ s; $T = 235$°C.

is seen in Figure 16. However, at values of D lower than a certain threshold of the order of 1×10^{-10} m^2/s, the diffusion-controlled regime sets in, the growth of the primary bubble becomes slower, and, as a result, the secondary nucleation decelerates and the duration of the devolatilization t^* increases, as is clearly seen in Figure 16.

It can be shown that the duration of the devolatilization process virtually does not depend on the initial concentration of the primary bubbles. Indeed, for example, for $\mu = 0.52\times 10^5$ Pa·s and $\lambda = 0.7$ s during a very short time $\Delta t = 0.07$ s growing secondary bubbles would be able to occupy a volume that is by two orders of magnitude larger than the initial volume. In the case of such flashlike secondary nucleation, an initial concentration of the primary bubbles does not effect significantly the process (assuming nevertheless that a nonzero concentration of the primary bubbles is given).

Conclusions

Experiments on polymer melt devolatilization demonstrated occurrence of foamed structures containing large voids. Secondary nucleation of stable nuclei (about 0.2 μm in radius) growing in the vicinity of a primary growing bubble was observed. Due to the fast simultaneous growth of the secondary bubbles, an entire neighborhood of the primary bubble disappears, resulting in a large void.

A new quantitative approach to the secondary bubble nucleation was developed, accounting for the elastic stresses and stored elastic energy in the vicinity of a primary bubble, which begins to grow when a sample is subjected to vacuum. The elastic energy accumulated is released due to mechanical degradation near the primary bubble. That promotes secondary nucleation in spite of the counteraction of the surface tension. Under certain conditions this secondary nucleation becomes flashlike, leading to rapid devolatilization of a sample.

The degree of devolatilization was predicted theoretically. We found a reasonable agreement between the theoretical results and the experimental data, although no adjustable parameters were involved.

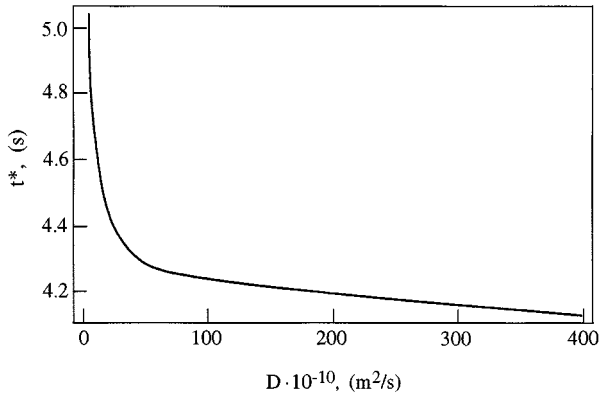

Figure 16. Effect of the diffusion coefficient on the duration of the devolatilization process at $T = 235$°C; $\lambda = 0.7$ s; $\mu = 10^5$ Pa·s.

Acknowledgment

The research was partially supported by the Technion V.P.R. Fund-P and E. Nathan Research Fund.

Literature Cited

Albalak, R. J., Z. Tadmor, and Y. Talmon, "Scanning Electron Microscopy Studies of Polymer Melt Devolatilization," *AIChE J.*, **33**, 808 (1987).

Albalak, R. J., Z. Tadmor, and Y. Talmon, "Polymer Melt Devolatilization Mechanisms," *AIChE J.*, **36**, 1313 (1990).

Biesenberger, J. A., and S. T. Lee, "A Fundamental Study of Polymer Melt Devolatilization: III. More Experiments on Foam-Enhanced Devolatilization," *Polym. Eng. Sci.*, **27**, 510 (1987).

Bird, R. B., W. E. Stewart, and E. N. Lightfoot, *Transport Phenomena*, Wiley, New York (1960).

Bird, R. B., R. C. Armstrong, and O. Hassager, *Dynamics of Polymeric Liquids*, Vol. 1, Wiley, New York (1977).

Blander, M., and J. L. Katz, "Bubble Nucleation in Liquids," *AIChE J.*, **21**, 833 (1975).

Doi, M., and S. F. Edwards, *The Theory of Polymer Dynamics*, Claredon Press, Oxford (1986).

Frenkel, J., *Kinetic Theory of Liquids*, Oxford Univ. Press, Oxford (1996).

Han, I. H., and C. D. Han, "Bubble Nucleation in Polymeric Liquids: I. Bubble Nucleation in Concentrated Polymer Solutions," *J. Poly. Sci. B*, **28**, 711 (1990a).

Han, I. H., and C. D. Han, "Bubble Nucleation in Polymeric Liquids: II. Theoretical Considerations," *J. Poly. Sci. B*, **28**, 743 (1990b).

Harvey, E. N., D. K. Barnes, W. D. McElroy, A. H. Whiteley, D. C. Peace, and K. W. Cooper, "Bubble Formation in Animals," *J. Cell Comp. Physiol.*, **24**, 1 (1944).

Landau, L. D., and E. M. Lifshits, *Theory of Elasticity*, Pergamon, London (1959).

Lastochkin, D. A., "Microstructure in Polymer Melt Devolatilization," PhD Thesis, Technion, Haifa, Israel (1998).

Leal, L. G., *Laminar Flow and Convective Transport Processes*, Butterworth, Boston (1992).

Lee, S. T., "Shear Effects on Thermoplastic Foam Nucleation," *ANTEC 91, SPE Tech. Papers*, **37**, 1304 (1991).

Lee, S. T., and J. A. Biesenberger, "A Fundamental Study of Polymer Melt Devolatilization: IV. Some Theories and Models for Foam-Enhanced Devolatilization," *Poly. Eng. Sci.*, **29**, 782 (1989).

Scriven, L. E., "On the Dynamics of Phase Growth," *Chem. Eng. Sci.*, **10**, 1 (1959).

Shulman, Z. P., and S. P. Levitsky, "Growth of Vapor Bubbles in Boiling Polymer Solutions: I. Rheological and Diffusional Effects," *Int. J. Heat Mass Transfer*, **39**, 631 (1996).

Skripov, U. P., *Metastable Liquids*, Wiley, New York (1974).

Stauffer, D., "Scaling Theory of Percolation Clusters," *Phys. Rep.*, **54**, 1 (1979).

Stauffer, D., *Introduction to Percolation Theory*, Taylor & Francis, London (1985).
Yang, C.-T., and T. G. Smith, "Polymer Trace Devolatilization: II. Case Study and Experimental Verification," *AIChE J.*, **43**, 1875 (1997).
Yarin, A. L., "Strong Flows of Polymeric Liquids: 1. Rheological Behavior," *J. Non-Newtonian Fluid Mech.*, **37**, 113 (1990).
Yarin, A. L., "Strong Flows of Polymeric Liquids: 2. Mechanical Degradation of Macromolecules," *J. Non-Newtonian Fluid Mech.*, **38**, 127 (1991).
Yarin, A. L., *Free Liquid Jets and Films: Hydrodynamics and Rheology*, Longman, Harlow and Wiley, New York (1993).
Zel'dovich, Ya. B., "On the Theory of New Phase Formation: Cavitation," *JETP*, **12**, 525 (1942); also *Selected Works of Ya. B. Zel'dovich*, Vol. 1, *Chemical Physics and Hydrodynamics*, Princeton Univ. Press, Princeton, NJ (1992).
Zel'dovich, Ya. B., "On the Theory of New Phase Formation: Cavitation," *Acta Physicochim. USSR*, **18**, 1 (1943).

Appendix

Summarize briefly the derivation of Zel'dovich (1942, 1943) leading to Eq. 25. Let the sizes of the nuclei of the secondary bubbles change due to thermal fluctuations in a discrete manner by jumps $\pm\Delta n$, where probability of the jump $+\Delta n$ is $q_+(n)$ and of the jump $-\Delta n$ is $q_-(n)$, where n is a current nucleus size. The number of the nuclei of size n, $Z(n)$, varies in time according to the equation

$$\frac{\partial Z(n)}{\partial t} = -Z(n)\left[q_+(n)+q_-(n)\right] + Z(n-1)q_+(n-1)+Z(n+1)q_-(n+1). \quad \text{(A1)}$$

Let $b(n)$ be an equilibrium number of the nuclei of size n, and thus

$$b(n)q_+(n) = b(n+1)q_-(n+1) \quad \text{(A2a)}$$

$$b(n-1)q_+(n-1) = b(n)q_-(n). \quad \text{(A2b)}$$

Exclude q_- from Eq. A1 using Eqs. A2, and denote from now on $q_+(n)$ simply $q(n)$. Then Eq. A1 takes the form

$$\frac{\partial Z(n)}{\partial t} = q(n)b(n)\left[\frac{Z(n+1)}{b(n+1)}-\frac{Z(n)}{b(n)}\right] - q(n-1)b(n-1)\left[\frac{Z(n)}{b(n)}-\frac{Z(n-1)}{b(n-1)}\right]. \quad \text{(A3)}$$

In the continuous description the probability density function corresponding to the nuclei with a size close to y is $f(y)$ having dimension (1/length). Therefore $Z(n)=lf(y)$, $Z(n+1)=lf(y+l)$, and so on. Note that the factor l stands for the dimensional reasons. Expanding all the functions involved in Eq. A3 in a series as l tends to zero, we reduce Eq. A3 to the following one:

$$\frac{\partial f}{\partial t} = \frac{\partial}{\partial y}\left[Db\frac{\partial}{\partial y}\left(\frac{f}{b}\right)\right], \quad \text{(A4)}$$

where D is the "diffusion" coefficient, $D=ql^2$.

In a stationary situation, when $\partial f/\partial t = 0$, we find from Eq. A4

$$Db\frac{\partial}{\partial y}\left(\frac{f}{b}\right) = C_1 \quad \text{(A5a)}$$

$$\frac{f}{b} = C_1\int_y^\infty \frac{dy}{Db} + C_2, \quad \text{(A5b)}$$

where C_1 and C_2 are the constants of integration.

At $y=\infty$ $f=0$, since the number of the nuclei larger than the critical one and continuing to grow is small, whereas at $y=0$ we have full equilibrium, and thus $f/b=1$. Using these boundary conditions, we obtain from Eq. A5b

$$\frac{f}{b} = \frac{\int_y^\infty (Db)^{-1}dy}{\int_0^\infty (Db)^{-1}dy}. \quad \text{(A6)}$$

The "flux" Fl of the nuclei over the size y-axis due to Eqs. A5a and A6 is given by

$$Fl = \left|Db\frac{\partial}{\partial y}\left(\frac{f}{b}\right)\right| = \frac{1}{\int_0^\infty (Db)^{-1}dy}. \quad \text{(A7)}$$

The "diffusion" coefficient D depends on y only slightly, since the probabilities of all the jumps are almost equivalent. Therefore D can be taken out from the integral in Eq. A7. On the other hand, the equilibrium number of the nuclei of size y depends on the free energy Φ, as usual as

$$b(y) \sim y_0 \exp\left[-\Phi(y)/kT\right], \quad \text{(A8)}$$

where $y_0 = x_0$, since the secondary nuclei are identical to the primary ones.

This expression can be expanded in a series, given the fact that Φ has a sharp maximum at the critical size of a stable nucleus y_{cr}. Therefore we have

$$b = b(y_{cr})\exp\left[-\frac{d^2\Phi}{dy^2}|_{y_{cr}}(y-y_{cr})^2\frac{1}{2kT}\right], \quad \text{(A9)}$$

where

$$d^2\Phi/dy^2|_{y_{cr}} < 0.$$

Substituting this expression in Eq. A7 and evaluating the integral $\int_0^\infty b^{-1}\,dy$, we obtain

$$Fl = \frac{Db(y_{cr})}{\sqrt{2\pi}}\sqrt{\left|\frac{d^2\Phi}{dy^2}\right|_{y_{cr}}/kT}. \quad \text{(A10)}$$

Considering viscous dissipation near a growing nucleus, Zel'dovich (1942, 1943) found that $D \sim kT/(\mu y_{cr})$. Substituting the latter and Eq. A8 into Eq. A10, and accounting for the three-dimensional character of the process, we find the rate of formation of the critical nuclei per unit volume, $I = Fl/x_0^4$, given by Eq. 25.

Manuscript received Mar. 1, 1999, and revision received July 14, 1999.